AD-A200 016

COMPUTATIONAL FLUID DYNAMICS

Proceedings of the International Symposium on
Computational Fluid Dynamics
Sydney, Australia, August 1987

Edited by

GRAHAM DE VAHL DAVIS

University of New South Wales
Kensington, New South Wales
Australia

and

CLIVE FLETCHER

University of Sydney
Sydney, New South Wales
Australia

DTIC
ELECTE
AUG 0 9 1988
S
H
D

N·H
C
1988

NORTH-HOLLAND – AMSTERDAM • NEW YORK • OXFORD • TOKYO

88 8 08 156

NAVIER-STOKES SIMULATIONS OF TIP VORTICES FOR FIXED AND ROTATING HELICOPTER BLADES*

G. R. Srinivasan

JAI Associates, Inc., Mountain View, California 94042, U.S.A.

W. J. McCroskey

U.S.Army Aeroflightdynamics Directorate-AVSCOM
NASA Ames Research Center, Moffett Field, California 94035, U.S.A.

Flowfield and tip vortex results are presented for hovering rotor blade at sub-critical and supercritical flow conditions for both nonlifting and lifting configurations. These results are calculated numerically by solving, in a time-accurate fashion, the unsteady thin layer Navier-Stokes equations written in rotor coordinates. The lifting calculations use an induced downwash correction,estimated from a free wake analysis, to the geometric angle of attack of the blades to account for the wake effect. Comparison of numerical results with the experimental data shows very good agreement for all cases considered. Alternate methods of calculating hovering rotor flowfield as steady state flowfield on isolated fixed-blade that have the same ciculation distribution as that of rotor in hover are explored. Comparison of these results with the rotor results indicate that centrifugal forces of the rotating blade have negligible influence on the overall flowfield at both subcritical and supercritical flow conditions. The results presented in this study are computed on a CRAY2 supercomputer.

1. INTRODUCTION

The need to accurately calculate the flowfield of a helicopter rotor in hover and forward flight is of great practical importance. Unlike the flowfield of a fixed wing, the flowfield of a helicopter rotor is generally more complex to analyze. The operating characteristics of a helicopter rotor are strongly influenced by the vortex wake. The interaction of this wake with the following blades is a potential source of unsteady lift fluctuation, noise and vibration under certain flight conditions. Accurate prediction of the vortical wake is probably the most important, most studied and the most difficult aspect of helicopter flowfield [1]. Current methods of analysis of wake range in complexity from relatively simple momentum-theory applications to free wake lifting surface methods. In between these extremes, there are a variety of so-called prescribed-wake models. Although such models are widely used in current prediction techniques, they suffer from the limitation that the empirical determination of the wake shape ignores some of the important details of the flowfield such as the mutual interaction between the vortex elements. Further, they are unreliable for unusual blade planforms and/or twist distributions which are often the case with the modern helicopter blade shapes.

Initially developed potential flow and Euler methods were primarily limited to calculating the nonlifting rotor flows because of the inherent limitation of not being able to model the vortex wakes with these equations, although the Euler formulation can model the vorticity transport correctly. These equation sets, which are inviscid in nature, basically lack the physical mechanism needed to model the tip vortex formation which involves the complex three-dimensional viscous flowfield in the tip region. At present the state of the Computational Fluid Dynamics (CFD) has matured to a stage where routine design calculations can be performed using the state-of-the-art codes, such as potential flow codes when coupled with proper wake model [2]. The thin layer Navier-Stokes simulations of tip-flows including tip vortices have been possible only recently after the faster and bigger supercomputers became available [3-4]. Understanding the mechanism of the tip vortex formation and subsequent roll-up would provide proper insight to modify the flow in the tip region and alleviate some of the problems caused by them. The ability to preserve and convect concentrated vortices in the finite difference grid without numerical diffusion [5] has been the biggest set back until now for much progress in simulating the wake and its induced effect on the rotor. However, the recently developed upwind schemes [6] and vortex-fitting schemes [7] in conjunction with a proper choice of either zonal grid or solution adapted grid show some promise to model the vortex wake. Even then the problem may be computer memory and CPU time dominated for use in routine design analysis. The use of Navier-Stokes codes to model the rotor flowfields have been limited in the past primarily because of this reason.

The object of the present investigation is to develop an unsteady, three- dimensional Navier-Stokes code to calculate the flowfield of a helicopter rotor in both hover and forward flight including the tip vortex formation and roll-up process in the wake. Simulation of tip vortex is only the first step in understanding the complex structure of wake flow. Alternate methods of calculating the hovering rotor flowfield in non-hover mode, like an isolated fixed-blade, keeping the circulation distribution same as that of the hovering blade, are also explored. Numerical results are compared with the availble experimental data.

2. GOVERNING EQUATIONS AND SOLUTION METHOD

The governing partial differential equations are the unsteady,thin-layer Navier-Stokes equations. For generality, these equations are transformed to an arbitrary curvilinear space (ξ, η, ζ, τ) retaining strong conservation law-form and are given by [8]

$$\partial_\tau \widehat{Q} + \partial_\xi \widehat{E} + \partial_\eta \widehat{F} + \partial_\zeta \widehat{G} = Re^{-1} \partial_\zeta \widehat{S} \tag{1}$$

where

$$Q = [\rho, \rho u, \rho v, \rho w, e]^T, \widehat{Q} = Q/J \tag{2}$$

and $\widehat{E}$, $\widehat{F}$, $\widehat{G}$ are convective flux vectors and $\widehat{S}$ is the viscous flux vector; J is the Jacobian of transformation, Re is the Reynolds number and the sign ^indicates that the quantity is normalised by J. The primitive variables of Eq. (1) are the density ρ, the three mass fluxes ρu, ρv and ρw in the three coordinate directions x, y and z, respectively and the energy per unit volume e. All these quantities are nondimensionlized by the appropriate free stream reference quantities.

The equation set given by Eq. (1) together with the equation of state for a perfect gas complete the set of equations that describe the flowfield. In the present approach, these equations are solved in the inertial reference frame. The inertial coordinates $\vec{X} = (x, y, z, t)$ are related to the blade fixed coordinates $\vec{X}_b = (\tilde{x}, \tilde{y}, \tilde{z}, \tilde{t})$ through the relation given by

$$\vec{X}(x,y,z) = \mathbf{R(t)}\vec{X}_b(\tilde{x},\tilde{y},\tilde{z}), t = \tilde{t} \tag{3}$$

where $\mathbf{R(t)}$ is the rotational matrix [9] given by

$$\mathbf{R(t)} = \begin{bmatrix} \cos\Omega\tilde{t} & -\sin\Omega\tilde{t} & 0 \\ \sin\Omega\tilde{t} & \cos\Omega\tilde{t} & 0 \\ 0 & 0 & 1 \end{bmatrix} \tag{4}$$

Here Ω is the reduced frequency of the rotor and Ωt represents the azimuth sweep of the rotor blade. In view of this relation, Eq. (4), the metrics in inertial reference frame are related in unsteady fashion to those in the blade-fixed frame of reference [10]. An implict, approximately-factored, partially flux-split numerical algorithm [11] is used to solve the governing equations. This numerical scheme uses spatial central differencing in the spanwise η and normal ζ directions and upwind differencing in the streamwise direction ξ and has option for first- or second- order time accuracy. Artificial numerical dissipation terms have been added in the central differencing directions for stability reasons. The factored operators are solved by sweeping in the ξ direction and inverting tridiagonal matrices in the other two directions. The numerical code is vectorized for the CRAY2 supercomputer.

A body conforming finite-difference grid has been used for the rectangular blade with a rounded-tip-capand consists of warped sperical O-O grid topology generated using a hyperbolic grid solver [12]. The grid has nearly 700,000 points and is well clustered in the leading edge and trailing regions as well in the tip region. It is nearly orthogonal at the surface with a spacing of 0.00006 in the normal direction. The grid boundary is 10 chords away in all directions.

The boundary conditions are applied explicitly. They consist of surface and farfield boundary conditions. For the rotating blade, the contravariant velocities are set zero for noslip condition at the surface but the time metrics ξ_t, η_t and ζ_t are nonzero. For the nonrotating blade, however, the contravariant velocities as well as the time metrics are zero at the surface. The pressure is determined from the normal momentum equation and the density is given by the adiabatic wall condition. At the farfield boundary the flow quantities are either fixed or extrapolated from the interior depending on whether the flow is subsonic or supersonic and if it is of inflow- or outflow-type. At the plane containing the blade root $\partial Q/\partial y = 0$ is imposed.

3. RESULTS

Results of both time accurate and time asymptotic (steady state) calculations are presented in this study for nonlifting rotor at $M_{tip} = 0.52$ and lifting rotor at $M_{tip} = 0.44$ and 0.877 and a geometric angle of attack of 8.0 degrees. The hovering calculations have been done in a time accurate manner and correspond to the conditions of a laboratory test on a two- bladed rotor in hover of Caradonna and Tung [13]. In this test, the rotor blade is an untwisted, untapered rectangular blade made up of NACA 0012 airfoil section. At the Reynolds numbers corresponding to the tip speeds in this test, the boundary layer can be assumed to be turbulent over the entire blade and Baldwin and Lomax algebraic turbulence model [14] is used to calculate the turbulent eddy viscosity. With a vecorized code for CRAY2 supercomputer, a typical solution required about 45-60 degrees of azimuth travel of marching for convergence with a CPU time per time step per grid point of about 8.5×10^{-5} sec.

3.1 Hovering Blade

Figure 1 shows the chordwise surface pressure distributions at several radial stations for a nonlifting rotor with a tip Mach number $M_{tip} = 0.52$ and the corresponding Reynolds number is 2.32 million. As seen the calculations are in excellent agreement with experimental data at all radial stations. For a lifting rotor, the induced effects of the wake have to be included to have a meaningful solution since the wake is not well resolved with the present approach. At present a number of methods are availble to model the effects of wake although most of them seem to give approximately the same kind of results when applied to a particular problem [2]. With this in mind, a uniform correction to the geometric angle of attack of the blade is used to include the wake effects. These estimates for the wake induced downwash are based on the calculations performed for the experimental rotor configuration by Agarwal and Deese [15] using a Free-Wake Analysis Program. Although an estimate of 3.8 degrees for the induced downwash for entire range of test conditions is good over a section of the blade along the radius, this value is assumed constant for the entire blade radius.
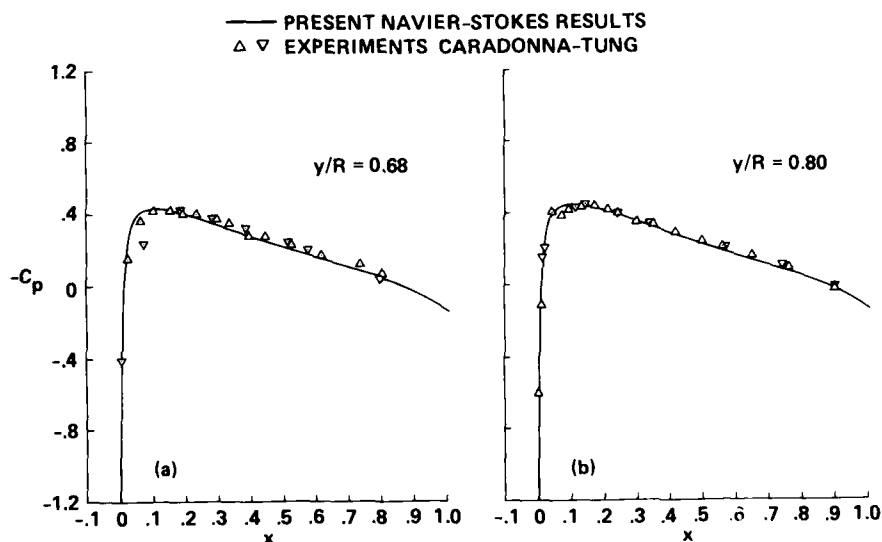

Fig. 1 Surface pressure distributions of a nonlifting rotor: $M_{tip}= ..52$, Re $= 2.32$ million.

The effective pitch θ of the lifting rotor is then the difference of the geometric angle of attack of the blade and the induced downwash. Lifting calculations have been performed using this estimate and Figs. 2 and 3 show representative results of these calculations compared with the experimental data. The comparison shows excellent agreement at least for the radial stations where the estimates of the induced downwash are nearly constant. The same flow has been calculated by Agarwal and Deese [15] using a finite volume Euler calculation in blade fixed coordinates. They also have good agreement with the experimental data for the pressures but the shock locations are over predicted in the supercritical case.
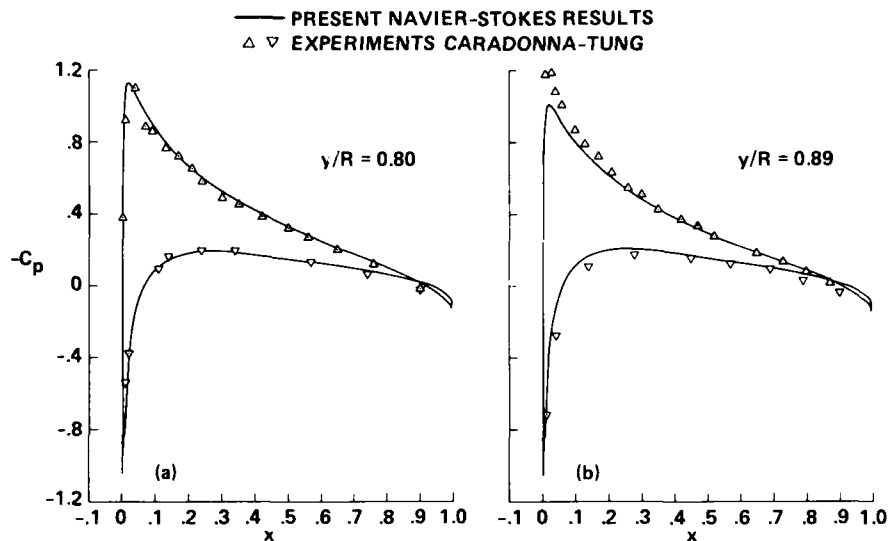
Fig. 2 Surface pressure distributions of a lifting rotor: $M_{tip} = 0.44$, Effective pitch = 4.2 deg., Re = 1.92 million.
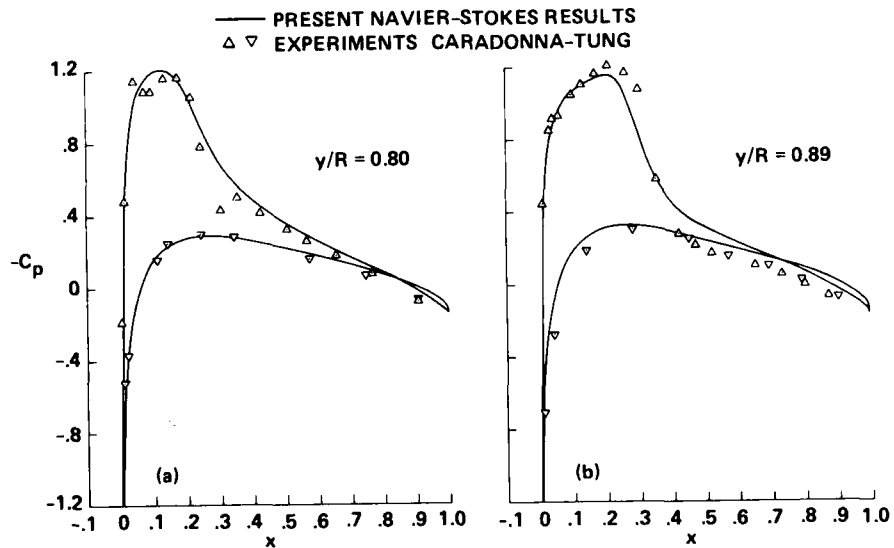

Fig. 3 Surface pressure distributions of a lifting rotor: $M_{tip} = 0.877$, Effective pitch = 4.2 deg., Re = 3.83 million.

3.2 Fixed Blade

This section explores alternate methods of calculating hovering blade flowfield in the blade-fixed configuration but having the same circulation distribution as that of a blade in hover. The objective is to examine the importance and role of centrifugal forces in the formation and roll-up of tip vortices. A clear understanding of this concept would be invaluable in guiding a design anlysis study of several exotic tip configurations both computationally and in the laboratory. Comparing the ciculation distributions for these two modes (fixed and rotating blades), one can conclude easily that there exists three different approaches with which this can be achieved, viz., a) have a Mach number distribution along the radius of the blade same as that of the rotating blade, b) keeping the Mach number constant along the entire blade radius and distributing a twist which decreases uniformly from tip to the root of the blade where the tip value is equal to the effective pitch of the rotating blade, and c) increasing the chord of the blade linearly from the root to the tip. This third option was not investigated in the present study.

With the above reasoning, steady state flowfields were calculated on the same (fixed) rectangular blades with the free stream conditions mentioned above. These calculations used a variable time step option suggested by Srinivasan et al [5] to accelerate the convergence rate. Figures 4 and 5 summarize these results in the form of surface pressure distributions for the subcritical and supercritical lifting cases. Comparison of these with the results for hovering blade shows surprisingly good agreement at the subcritical condition for both options of variable twist, $\theta(y)$, and variable Mach number, $M_\infty(y)$ as shown in Fig. 4. At the supercritical condition, however, the flowfield for the option of variable twist is dominated by strong transonic shock, but the variable Mach number option is generally in good agreement with the hover results. The variable twist option does not seem to perform as well in the transonic regime. This is not surprising since high flow Mach number, equal to tip Mach number, exists all along the span for this non-rotating blade.
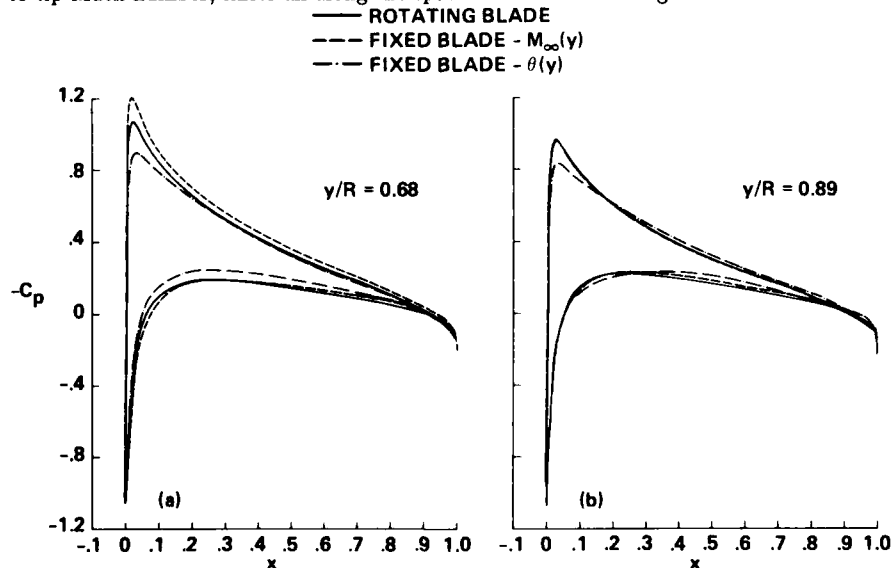

Fig. 4 Comparison of surface pressure distributions for fixed and rotating lifting blade: $M_{tip} = 0.44$, $\theta_{tip} = 4.2$ deg., Re = 1.92 million.
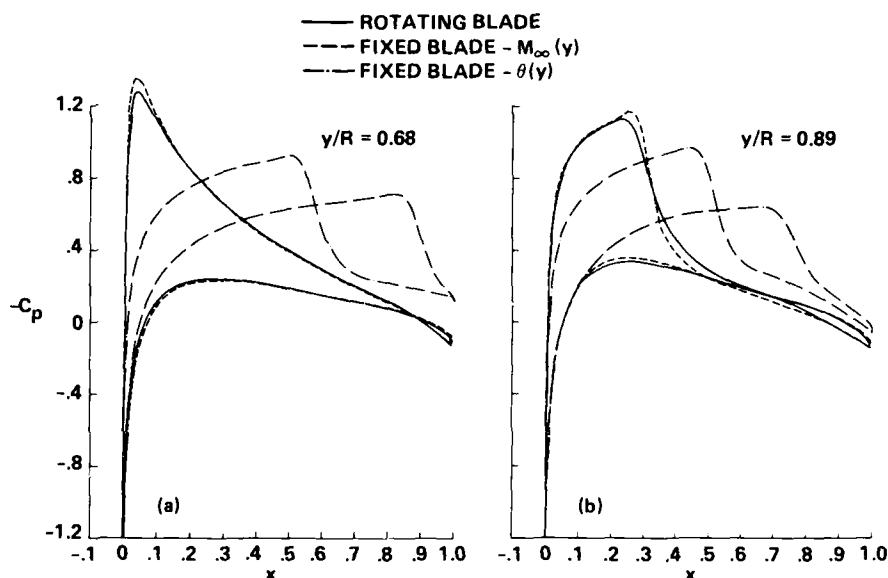
Fig. 5 Comparison of surface pressure distributions for a fixed and rotating lifting blade: $M_{tip} = 0.877$, $\theta_{tip} = 4.2$ deg., Re $= 3.83$ million.

Considering close agreement of the results for the variable Mach number option at both subcritical and supercritical conditions, even at the radial stations close to the tip region, it appears that the influence of centrifugal forces of the rotating blade have very little effect in modifying the pressure field even in the tip region as is apparent also from the surface pressure contour plots shown in Fig. 6. There are small differences in the flow near the surface, however, as is apparent from the surface particle flow pictures of Fig. 7. The variable twist option produced strong shocks on both sides of the wing and its surface pressure distribution is very different from that of the variable Mach number case as seen from Figs. 6b and 6c. Inspite of these differences, the (near) surface flow in the tip region for these two appear to be similar as seen in Figs. 7b and 7c. The rotating blade shows small local separation on the face of the tip (see Fig. 7a) but this appears to have negligible influence on the surrounding pressure field as is apparent from Figs. 6a and 6b. In Fig. 7 the surface particle flow is simulated by releasing the flow particle tracers at one grid point above the surface and constraining it to stay in that plane. This method is supposed to mimic surface oil flow visualization.

In contrast, the tip vortex formation and roll-up shown in Fig. 8 uses particle tracers released at different heights from the surface and at several spanwise locations. Examination of these particle traces reveal that the process of formation of tip vortex which involves braiding of fluid particle traces from the lower surface (high pressure side) of the wing crossing over the tip to the upper surface (low pressure side) starts early for the fixed blade configurations of Figs. 8b and 8c compared to the rotating blade for which this process is delayed until after the formed vortex on the upper surface lifts-off from the surface as is apparent in Fig. 8a. The possible reason may be that the lift-off of the vortex for the rotating blade occurs inboard of the tip on the upper surface, where as for the fixed-blade configurations lift-off occurs right on the tip. Figure 8 also shows how these tip vortices
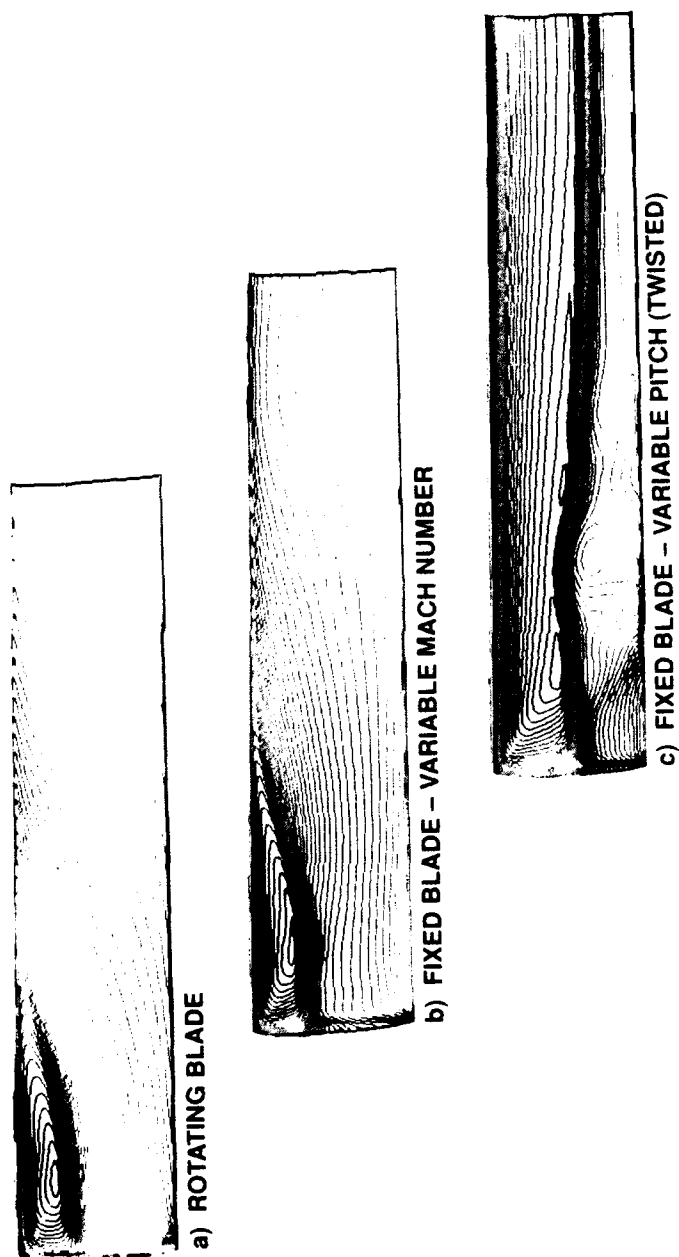
G.R. Srinivasan and W.J. McCroskey

a) ROTATING BLADE

b) FIXED BLADE – VARIABLE MACH NUMBER

c) FIXED BLADE – VARIABLE PITCH (TWISTED)

Fig. 6 Surface pressure contour plots for rotating and fixed blades: $M_{tip} = 0.877$, $\theta_{tip} = 4.2$ deg., Re $= 3.83$ million.

a) ROTATING BLADE

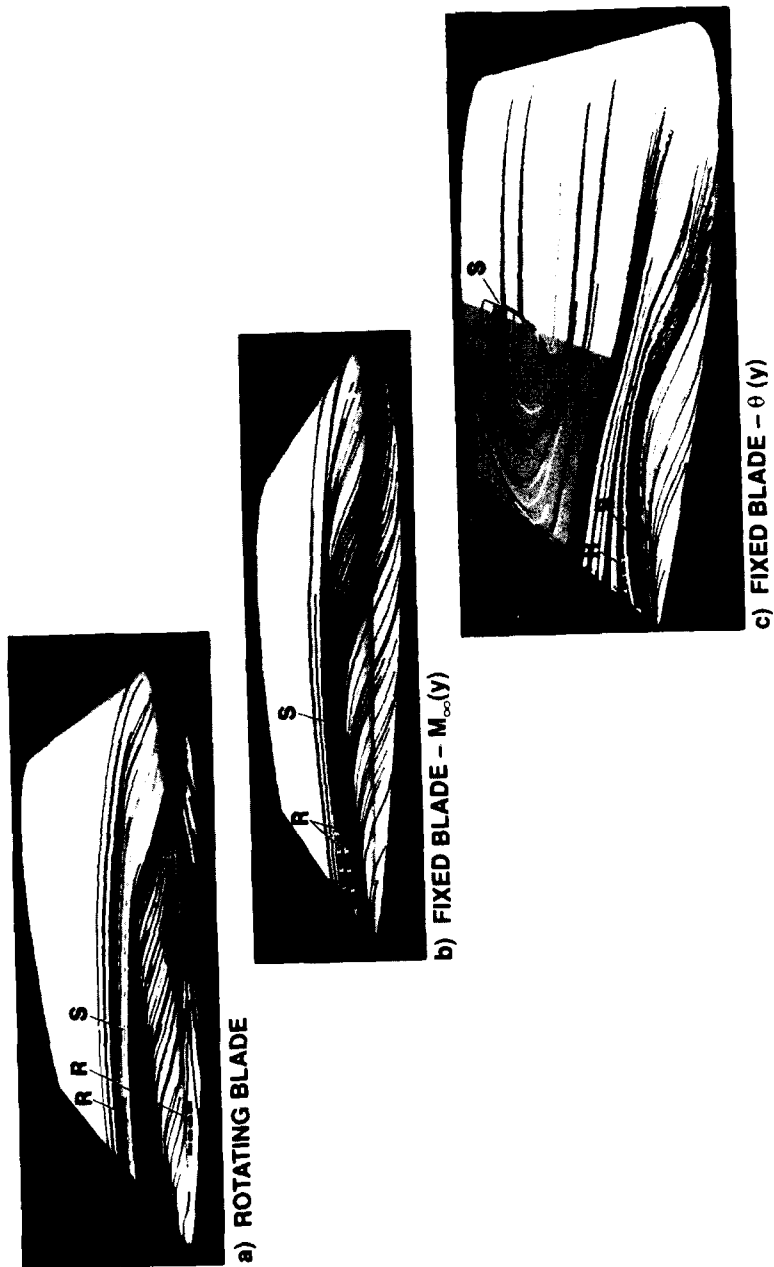b) FIXED BLADE – $M_\infty(y)$

c) FIXED BLADE – θ (y)

Fig. 7 Surface particle flow traces in the tip region of rotating and fixed blades: $M_{tip} = 0.877$, $\theta_{tip} = 4.2$ deg., Re = 3.83 million.
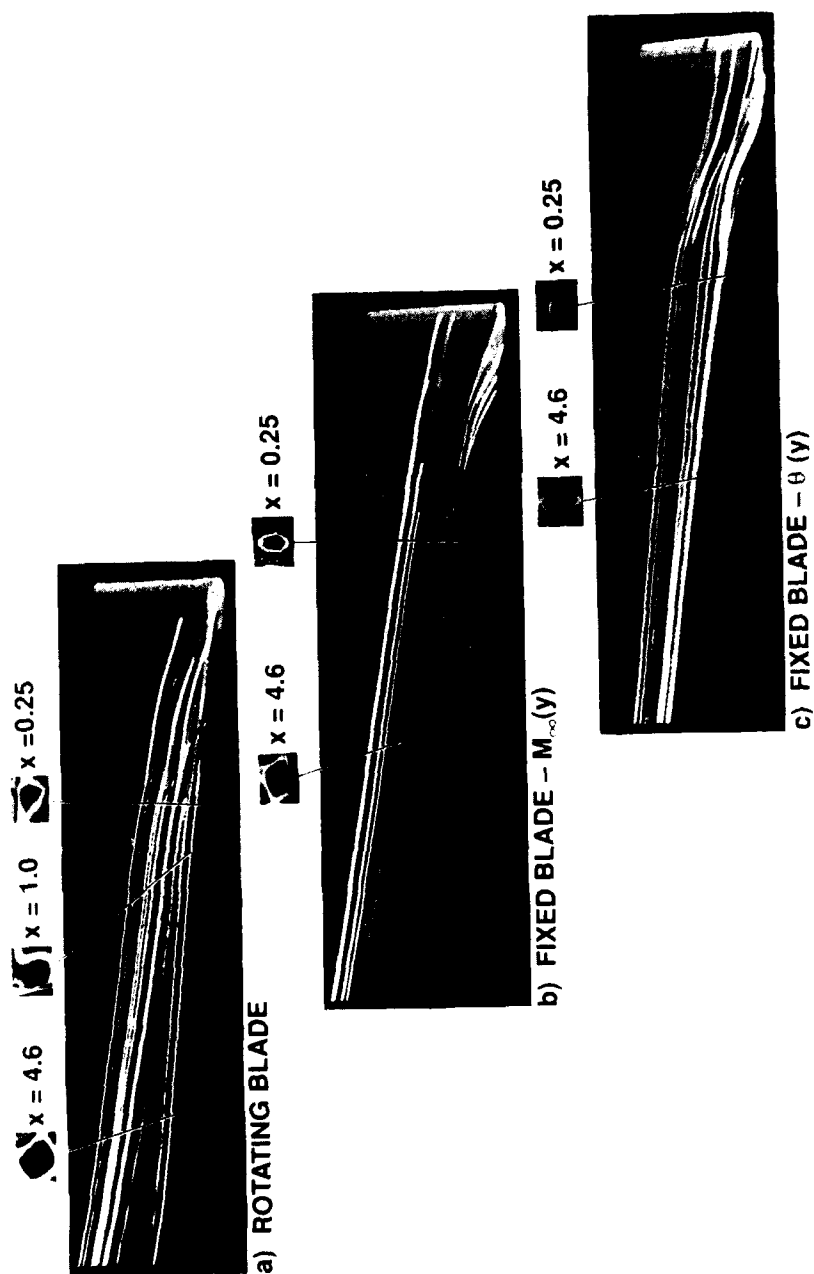
Fig. 8 Far-field view of tip vortics of rotating and fixed blades: $M_{tip} = 0.877$, $\theta_{tip} = 4.2$ deg., Re = 3.83 million.

while in roll-up process also roll inboard and stay distinctly above the wake vortex sheet. The vorticity contours shown in inserts in this figure give the approximate shape and size of these vortices. Estimation of tip vortex strengths based on the line integral of the velocity vector around a closed path enclosing the vortices gave almost identical values for the rotating and fixed-blade variable Mach number case of 0.07-0.08 for which the integrated value of lift coefficient is 0.17. The variable twist case produced much stronger vortex, approximately 2.5 times that of the hovering blade value. It should be emphasized that all calculations, both time accurate and steady state, were done on the same grid topology to remove any grid dependency from the comparisons.

4. CONCLUSIONS

A procedure to calculate the unsteady, viscous flowfield of a hovering rotor in an inertial reference frame has been developed based on the solution of thin layer Navier-Stokes equations using a partially flux-split numerical algorithm of Ying and Steger [11]. The numerical results for both nonlifting and lifting hovering rotor compare very well with the experimental data of Caradonna and Tung [13]. For lifting calculations, the induced wake effects have been considered as a correction to the geometric angle of attack of the blade. Methods to calculate the hover flowfield in blade-fixed mode showed that in the subcritical case, either option of variable twist or variable Mach number would produce nearly the same flow as that of a hovering blade. In the supercritical case, however, only the variable Mach number option seem to produce flowfield that is close to the hovering blade flowfield. In cases where the flowfield on the fixed blade is nearly identical to that on the hovering blade, the influence of centrifugal forces of the rotating blade appears to be negligible. While this conclusion is primarily based on the comparisons of surface pressures and vortex strength estimates, further quantitative comparison of the vortex structure is needed for a clear understanding of the similarities and differences.

REFERENCES

[1] McCroskey, W. J., "Special Opportunities in Helicopter Aerodynamics" in: Krothapalli, A. and Smith, C. A., (eds.), Recent Advances in Aerodynamics (Springer-Verlag, New York, 1986) pp. 721-752.

[2] Caradonna, F. X. and Tung, C., "A Review of Current Finite Difference Rotor Flow Codes", *Proceedings of the 42nd Annual Forum of the American Helicopter Society*, (1986), pp. 967-983.

[3] Srinivasan, G. R., McCroskey, W. J., Baeder, J. D. and Edwards, T. A., "Numerical Simulation of Tip Vortices of Wings in Subsonic and Transonic Flows", AIAA Paper No. 86-1095, 1986.

[4] Mansour, N. N., "Numerical Simulation of Tip Vortex off a Low-Aspect Ratio Wing at Transonic Speed", *AIAA Journal*, Vol. 23, 1985, pp. 1143-1149.

[5] Srinivasan, G. R., Chyu, W. J. and Steger, J. L., "Computation of Simple Three-Dimensional Wing-Vortex Interaction", AIAA Paper No. 81-1206, 1981.

[6] Rai, M. M., "Unsteady Three-Dimensional Navier-Stokes Simulations of Turbine Rotor-Stator Interaction", AIAA Paper No. 87-2058, 1987.

[7] Srinivasan, G. R. and McCroskey, W. J., "Numerical Simulations of Unsteady Airfoil-Vortex Interactions", *VERTICA*, Vol. 11, 1987, pp. 3-28.

[8] Pulliam, T. H. and Steger, J. L., "Implicit Finite-Difference Simulations of Three-Dimensional Compressible Flow", *AIAA Journal*, Vol. 18, 1980, pp. 159-167.

[9] Isom, M. P., "Unsteady Subsonic and Transonic Potential Flow over Helicopter Rotor Blades", NASA CR-2463, October 1974.

[10] Srinivasan, G. R. and McCroskey, W. J., "Navier-Stokes Calculations of Hovering Rotor Flowfields", AIAA Paper No. 87-2629-CP, 1987.

[11] Ying, S. X., Steger, J. L., Schiff, L. B. and Baganoff, D., "Numerical Simulation of Unsteady, Viscous, High-Angle-Of-Attack Flows Using a Partially Flux-Split Algorithm" AIAA Paper No. 86-2179, 1986.

[12] Steger, J. L. and Chaussee, D. S., "Generation of Body-Fitted Coordinates Using Hyperbolic Partial Differential Equations", SIAM J. Sci. Stat. Comput., Vol. 1, 1980, pp 431-437.

[13] Caradonna, F. X. and Tung, C., "Experimental and Analytical Studies of a Model Helicopter Rotor in Hover", NASA TM-81232, September 1981.

[14 Baldwin, B. S. and Lomax, H., "Thin Layer Approximation and Algebraic Model for Separated Turbulent Flow," AIAA Paper No. 78-257, 1978.

[15] Agarwal, R. K. and Deese, J. E., "Euler Calculations for Flowfield of a Helicopter Rotor in Hover", AIAA Paper No. 86-1782, 1986.